ELSEVIER

Contents lists available at ScienceDirect

# Chemical Engineering Journal

journal homepage: www.elsevier.com/locate/cej



# Efficient light-driven charge storage in titania aerogels: From photochemical batch studies to capillary flow reactors

Akbar Valaei<sup>a,1</sup>, Anja Hofmann<sup>b,1</sup>, Alexandra Rose<sup>c</sup>, Paul Kuschmitz<sup>c</sup>, Pascal Voepel<sup>c</sup>, Barbara Milow<sup>c</sup>, Roland Marschall<sup>b,\*</sup>, Dirk Ziegenbalg<sup>a,\*</sup>

#### ARTICLE INFO

#### Keywords: Light-harvesting Photocharging Batch-to-conti Photoreactor scale-up Radiation field characterization

#### ABSTRACT

A major challenge in photocatalyst design is separating light-harvesting from catalytic steps, for which photochargeable materials provide a promising approach for decoupling light-driven energy storage from subsequent dark reactions. This work systematically investigates the exceptional capability of as-synthesized titania aerogels to store electrons upon irradiation, including sacrificial agents, irradiation time, and incident photon flux. Methanol, owing the highest number of  $\alpha$ -H atoms, was the most effective sacrificial agent compared to ethanol and isopropanol, enabling electron storage up to  $64.8 \, \mu mol \, e^-$  in  $100 \, mg$  titania aerogel. Moreover, insights from studies in a semi-batch reactor (Xe-arc lamp) were translated to a flow capillary reactor irradiated with UVA LEDs. A characterization of the radiation field of both reactors allowed for an objective comparison of data obtained in the different experimental setups. Using the same charging conditions in the capillary reactor as in the semi-batch reactor yielded a low charging performance, due to a significant light transmission loss caused by low loading. Photocharging conditions were tailored to account for the short optical path length of the capillary reactor by an increase of the titania aerogel loading and a reduced dispersion volume. This enhanced the photocharging rate in the capillary reactor, eventually exceeding that of the batch system by a factor of two. Doubling the catalyst loading increased photonic efficiency fourfold, demonstrating both the potential and challenges of transferring and scaling light-driven processes from batch to flow, and establishing critical design insights for light-driven charge storage in continuous systems.

# 1. Introduction

 ${\rm TiO_2}$  is one of the most investigated photocatalysts [1–12]. Among the different types of  ${\rm TiO_2}$ ,  ${\rm TiO_2}$  aerogels are particular attractive as these materials possess a high number of reactive sites, resulting from the high surface areas, improved charge carrier separation, and short diffusion pathways for minority charge carriers, all of these properties being crucial for efficient photocatalysis [8,9,13]. Aerogels are characterized by an interconnected porous network with open pores, low densities, and high surface areas [14,15]. For example, the surface areas for amorphous  ${\rm TiO_2}$  aerogels are of up to more than 700 m<sup>2</sup> g<sup>-1</sup> [6,16–19]. The properties of aerogels can be tailored by adjusting the synthesis parameters and post-synthesis processing [6,16,17,20].

Compared to TiO<sub>2</sub> nanoparticles, the photogenerated electron-hole pairs in TiO<sub>2</sub> aerogels are more efficiently separated and the density of excited electrons is enhanced [8]. Another advantage of TiO<sub>2</sub> aerogels, especially of amorphous/semi-crystalline TiO<sub>2</sub> aerogels, compared to nanoparticulate systems is their increased electron storage capability [6], which is advantageous for the use as a solar battery material. Electrons in TiO<sub>2</sub> are trapped close to the surface in the presence of a hole scavenger, forming Ti<sup>3+</sup> states that exhibit a characteristic dark blue coloration, *i.e.* a broad absorption at a maximum of 650 nm [6,21–24]. Thereby, very small concentrations of a hole scavenger, *i.e.* 0.02 mol L<sup>-1</sup> ethanol, are already enough for the extraction of the photoexcited holes and the storage of the photoexcited electrons in the TiO<sub>2</sub> [25]. These photogenerated stored electrons can be used for reduction reactions of

E-mail addresses: Roland.marschall@uni-bayreuth.de (R. Marschall), Dirk.ziegenbalg@uni-ulm.de (D. Ziegenbalg).

<sup>&</sup>lt;sup>a</sup> Institute of Chemical Engineering, Ulm University, Albert-Einstein-Allee 11, 89081 Ulm, Germany

<sup>&</sup>lt;sup>b</sup> Department of Chemistry, University of Bayreuth, Universitätsstraße 30, Bayreuth 95447, Germany

<sup>&</sup>lt;sup>c</sup> German Aerospace Center, Institute for Frontier Materials on Earth and in Space, Department of Aerogels and Highly Porous Materials, Linder Höhe, 51147, Cologne, Germany

<sup>\*</sup> Corresponding authors.

Both authors contributed equally

different metal ions, e.g. silver [22], gold [23], cupper [25], or platinum ions [6], or for the reduction of other electron donors in the dark [26–28]. One very promising reduction reaction, which was shown for the first time by Bahnemann et al. in 2011, is the nitrogen reduction reaction to ammonia in the dark with these stored electrons in  $\text{TiO}_2$  [25]. Marschall et al. showed that as-synthesized  $\text{TiO}_2$  aerogels exhibit the best capability to store photoexcited electrons compared to aerogels, which were calcined at 300, 400, and 500 °C. It could also be shown that these photostored electrons in the as-synthesized  $\text{TiO}_2$  aerogel are able to reduce nitrogen to ammonia in the dark [6]. Other reduction reactions for the synthesis of ammonia using photostored electrons in  $\text{TiO}_2$  are the nitrate or the nitric oxide reduction reactions [25,29,30].

Sustainable processes using stored electrons can become a very important tool for the future economy and can pave the way for an energy-efficient and decentralized production of solar fuels, *i.e.* ammonia. For such reactions, it is important to quantify the amount of photostored electrons in the material, which are available for the following reduction reaction after the photocharging. The quantification of photostored electrons in  $\text{TiO}_2$  can be done with different approaches, *e.g.* by titration with methylene blue [28,31] or by the addition of a given amount of  $\text{Pt}^{4+}$  to the photocharged  $\text{TiO}_2$  and the high-resolution detection of the evolved hydrogen [6].

To drive commercial adoption of photocatalysis, pivotal advancement is needed in photochemical reaction engineering. Standardized metrics for reports play a crucial role in simplifying the evaluation of photocatalysts since it removes bias and helps to generate reproducible results. This can expedite materials screening for commercialization, addressing a persistent challenge in the field: the lack of detailed and consistent documentation of experimental setups [32-34]. However, beyond materials evaluation, designing scalable, efficient, and userfriendly photoreactors remains a critical bottleneck for large-scale implementation of photocatalytic processes across numerous applications [35,36]. This challenge primarily arises from the exponential light intensity attenuation within photoreactors, which must to be considered in conjugation with mass and heat transfer phenomena [37,38]. In this regard, photonic characterization of photoreactors becomes essential. Detailed characterization provides critical insights into design limitations and opportunities for improvement. Sender et al. [39,40] proposed a radiometric scanning method to evaluate the radiation field within photoreactors. Applying this technique to different configurations of photoreactor enables to gain a deeper understanding of the impact of design decisions on the photonic efficiency.

Despite the recent developments in photoreactor design and photocatalyst, the connection between photoreactor design and photocatalytic performance remains inadequately understood. In this work, the exceptional light-induced electron storage capabilities of assynthesized TiO<sub>2</sub> aerogels were investigated for different parameters. Subsequently, two reactor configurations, a semi-batch reactor and a capillary reactor, were compared based on the radiation fields by characterizing light sources and using radiometric scanning. This integrated approach allowed a direct connection between reactor design, photonic efficiency, and photocatalystic performance of the material.

# 2. Experimental

#### 2.1. Chemicals

Titanium(IV) tetraisopropoxide (98 %, Merck), hydrochloric acid (37 %, ACS reagent, Sigma-Aldrich), ethanol (CHEMSOLUTE, denatured with MEK, IPA, and Bitrex, 99.8 %), methanol (99.9 %, Fisher Chemical), ethanol (VWR, 99.9 %), isopropanol (VWR, >99 %), hexachloroplatinate(IV) hydrate (99.995 %, Carl Roth), and Hombikat UV 100 (99 %, Sachtleben Chemie) were used as received.

#### 2.2. Synthesis of TiO2-aerogel

The TiO<sub>2</sub> aerogel used herein was synthesized as previously reported by a HCl-catalyzed sol-gel method without further thermal treatment after the supercritical drying using scCO<sub>2</sub> [6].

#### 2.3. TiO2-aerogel characterization

XRD measurements were conducted on a Bruker D8 ADVANCE X-ray diffractometer using a Cu  $K_{\alpha}$  radiation source and a LYNXEYE XE-T detector. The diffraction data were measured in the range of 15–90°  $2\theta$  with a step size of  $0.01^{\circ}$ . The crystallite sizes were estimated using Bruker EVA software by calculating the integral breadth from the XRD pattern. Phase quantification and determination of the amorphous and crystalline phase was performed using the Rietveld method implemented in Topas with CeO $_2$  as the internal standard.

The specific surface area was determined  $via~N_2$  physisorption measurements at 77 K on a Micromeritics 3Flex instrument in a partial pressure range of  $0.05 < p/p^0 < 0.3$  using the Brunauer–Emmett–Teller (BET) method. The total pore volume of the samples was obtained from the  $N_2$  desorption isotherms at a partial pressure of 0.98, and the pore size distribution was obtained using the Barrett–Joyner–Halenda (BJH) model. Prior to physisorption analysis, the samples were degassed at 60 °C for 12 h on a Micromeritics VacPrep Gas Adsorption Sample Preparation Device.

#### 2.4. Semi-batch reactor setup

Measurements of the photocharging were performed in two different reactor setups. Fig. S1 in the Supporting Information (SI) shows the semi-batch reactor setup, which was used also in previous work. In this reactor setup, the carrier gas can be switched between argon and nitrogen. For the measurements, a top irradiation batch reactor is used, which is equipped with a fixed quartz glass slide on the top with 5 cm in diameter and which can be cooled by a thermostat from Lauda (ECO RE1050G). A continuous gas-flow is used, which can be adjusted with a mass flow controller from Bronkhorst. The gas stream behind the reactor is heated to 110 °C and guided into a drying column equipped with silica gel. The gas evolution can be detected online either by a gas chromatograph (GC, GC2014 from Shimadzu), equipped with a shin carbon ST column (Restek) and a thermal conductivity detector, using argon 5.0 as the carrier gas, or by a mass spectrometer (MS, Hiden HPR-20 Q/C from Shimadzu) using either argon 5.0 or nitrogen 5.0 as carrier gas.

# 2.5. Capillary reactor setup

A custom-made capillary reactor was used for investigating the photocharging of the as-synthesized titania aerogel in a flow reactor. This photoreactor consists of two layers of capillaries wound in a spiral shape (Fig. 1). A scaffold holds capillaries and LEDs as light sources. The scaffold is 3D-printed from polylactic acid (PLA) using a Raise Pro2 Plus printer (Raise3D Premium PLA Filament and extrusion temperature of 205  $^{\circ}$ C). The holder, with an inner diameter of 15 cm, was designed to arrange the two layers of capillaries with an offset of one capillary diameter (see Fig. S2c). This offset is intended to ensure that the gap between adjacent capillaries is properly filled, optimizing the alignment and structural integrity within the reactor system. Details of the design are shown in the supplementary information (Figs. S3-S5). 4 LEDs (365 nm, Luminus LST1-01G01-UV01-00, Luminus Devices, Inc.) were positioned on each side of the holder in a circular pattern at 90-degree intervals. On the upper side of the reactor, the first LED was placed at an angle of 0 degree, while the first LED on the lower side of the reactor was rotated by 45 degrees to increase the homogeneity of photon irradiance (see Fig. 1 and Fig. S5). The spiral design of the capillary guarantees extended irradiation times. The total length of the capillary used in the system was 9 m. Polymeric capillaries with 1/8" outer diameter

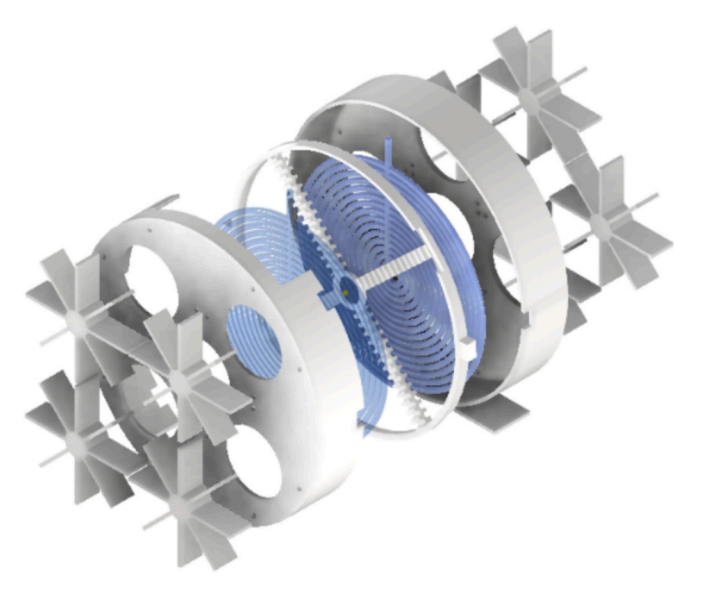


Fig. 1. Configuration of the capillary photoreactor designed in this work.

and 1/16'' inner diameter made from different materials, including perfluoro alkoxy alkane (PFA, Bohlender GmbH, Germany), fluorinated ethylene propylene (FEP, Bohlender GmbH, Germany), and polyvinylidene fluoride (Kynar Flex<sup>TM</sup> 2750 PVDF) were evaluated as reactor material.

#### 2.6. Reaction engineering investigations in the semi-batch reactor setup

The dependence of the photocharging of the aerogel on the sacrificial agent, light intensity, and irradiation time was determined by quantification of the amount of stored electrons with the reduction of Pt<sup>4+</sup> to Pt<sup>0</sup> in the dark, as reported previously [6]. For all measurements 100 mg of the as-synthesized aerogel was dispersed in 150 mL of a 10 vol% aq. alcohol solution and the temperature was set to 20 °C using a Lauda thermostat (ECO RE1050G). The dispersion was stirred and the reactor was flushed with Ar 5.0 for 1~h with 100~mL min $^{-1}$  (set with a Bronkhorst mass flow controller) to remove all residues of air in the reactor. The flow was reduced to 25 mL min<sup>-1</sup> Ar and the gas evolution was detected online for 30 min with a GC (GC2014 from Shimadzu, equipped with a shin carbon ST column (Restek) and a thermal conductivity detector, using argon 5.0 as the carrier gas) every 10 min and then the sample was irradiated with a 300 W Xe lamp (Quantum Design). After a certain time, the lamp was switched off and for around 20 min measurements were still performed with the GC before the detection was switched to the high-resolution detection with MS every 12 s. For this, the flow was increased to 100 mL min<sup>-1</sup> Ar and it was waited for stable H<sub>2</sub> evolution. Subsequently, an aqueous solution of H<sub>2</sub>PtCl<sub>6</sub> was added to reach a concentration of 0.1 wt% Pt and the H<sub>2</sub> evolution peak was detected in the dark.

Small variations were implemented to investigate the dependence of the photocharging on the different parameters:

For the dependence of the photocharging on the sacrificial agent, either 150 mL 10 vol% aq. alcohol solution of absolute methanol, ethanol, or isopropanol were used and the irradiation time for all measurements was 110 min with a 300 W Xe lamp operated without filter.

For studies on the dependence on the light intensity, a 10 vol% aq. alcohol solution of methanol was used, and the irradiation time was set to 110 min for all measurements with a 300 W Xe lamp. Measurements were performed without a filter, with a ND0.10 filter (79.4 % transmission), with a ND0.20 filter (63 % transmission), with a ND0.40 filter (39.8 % transmission), or with a ND0.70 filter (20 % transmission) from Quantum Design. The lamp spectra without and with the different filters

were measured with a Flame spectrometer from Ocean Insight and are shown in Fig. S6.

For the dependence on the irradiation time, a 10 vol% aq. alcohol solution of methanol was used and the irradiation time with a 300 W Xe lamp was set to either 10 min, 20 min, 50 min, 80 min, 110 min, 4 h, 6 h, or 12 h of irradiation.

#### 2.6.1. Cycling test

For the cycling test, the same conditions were used as described above with a 10 vol% aq. alcohol solution of methanol. The dispersion was irradiated for 110 min with a 300 W Xe lamp, then the lamp was switched off, the hydrogen evolution rate was detected with the GC until the rate of evolved hydrogen became much smaller than in the beginning after the lamp was switched off. After that, the lamp was switched on again and the sample was irradiated for another 110 min. This cycle was repeated seven times, and it was waited until the hydrogen evolution became nearly zero in the last step.

#### 2.6.2. Charging persistence test

For the test of the persistence of the charging state of the aerogel, the same conditions were used as described above with a 10 vol% aq. methanol solution. The dispersion was irradiated for 110 min with a 300 W Xe lamp, then the lamp was switched off and the hydrogen evolution rate in the dark was detected with the GC until no hydrogen evolution was detected anymore. Furthermore, photographs of the dispersion were taken before the irradiation, after 110 min of irradiation, and at different times after the irradiation until the dispersion became colorless again as in the beginning of the experiment.

#### 2.7. Photocharging experiments using the capillary reactor

To study the photocharging of titania in the capillary reactor, 100 mg of as-synthesized aerogel (particle size less than 63 µm) was dispersed in 10 vol% aqueous alcohol solutions, consisting of 135 mL water and 15 mL absolute alcohol. If not stated otherwise, methanol was used. Ar was bubbled through the mixture to remove all residues of oxygen until oxygen could not be detected anymore with the attached microGC (DynamiQ-S from qmicro equipped with TCD detector and WCOT/PLOT columns). A SIMDOS 10 pump manufactured by KNF was used to circulate the TiO<sub>2</sub> dispersion in the capillary reactor. The sample was irradiated for 3 h with UV-LEDs (365 nm) while pumping the mixture through the reactor with a flow rate of 10 mL min<sup>-1</sup>. The flow diagram of the setup is shown in Fig. S7 in the SI. After photocharging, light was turned off and the hydrogen produced during the photocharging was purged from the reservoir. Subsequently, 1 mL of an aqueous H<sub>2</sub>PtCl<sub>6</sub> solution was injected in the reservoir, using a syringe pump and the GC operation was changed to high-resolution detection to measure the hydrogen evolution peak in the dark. A measurement of hydrogen was done every 14 s.

# 2.8. Radiation field characterization

Radiometric scans were done using the multidimensional radiometric setup developed by Sender et al. [39,40] The setup equipped with a UV–Vis spectrometer measures light intensity across a two-dimensional plane above the photoreactor. The detector is fixed on a computer controlled motorized X/Y-translation stage. This system allows to position the spectrometer across the plane and measure the full light spectrum at each grid point. The integration time is adjusted automatically to avoid saturation. The collected spectra are post-processed to generate two-dimensional heat maps that visually represent the irradiance distribution. For the capillary reactor used in this study, scans were conducted under various conditions: with the light sources alone, with the light sources installed in the reactor, with the reactor containing capillaries filled with water-methanol, and with the reactor filled with a concentrated methyl orange solution (5 g  $L^{-1}$ ).

Concentrated methyl orange was employed to ensure complete UV absorption, allowing accurate quantification of photons.

#### 2.9. Integrating sphere measurements

The radiometric output of the UV-LEDs was measured using a calibrated integrating sphere (Mountain Photonics GmbH, Landsberg am Lech, Germany) to determine the integral radiant flux. An AvaSpec-ULS2048CL-EVO-RS-UA spectrometer (Avantes, The Netherlands), calibrated for this setup by Mountain Photonics GmbH, was employed for spectral measurements. These measurements were used to calibrate the radiometric scans of the sole LEDs to ensure accurate quantification of the photon flux entering the reactor. Detailed information on the measurements are provided in the SI.

# 2.10. Extinction coefficient measurement

The absorbance of the photocatalyst was measured as a function of photocatalyst loadings in a methanol-water mixture using various optical path lengths (0.2, 0.5, 1, 2, and 5 cm). These cuvettes were securely positioned using custom 3D-printed holders; the corresponding CAD designs are available [41]. Titania aerogel was dispersed in a 10 % V/V aqu. methanol solution using an ultrasonic bath, resulting in a stable suspension for several minutes. Light absorption at 365 nm was then measured for each cuvette and extinction coefficient was determined by applying Beer-Lambert law.

#### 3. Results and discussion

The used as-synthesized  $\rm TiO_2$  aerogel is semi-crystalline with 10 % crystalline phase (anatase) and 4 nm crystallite size, which is in accordance to our previous publication. Anatase is the only occurring crystalline phase after calcination [6]. The corresponding  $\rm N_2$  isotherm and pore size distribution of the used as-synthesized  $\rm TiO_2$  aerogel is shown in Fig. S8. The aerogel exhibits a surface area of 642 m<sup>2</sup> g<sup>-1</sup>, a cumulative pore volume of 2.6 cm<sup>3</sup> g<sup>-1</sup> and an average pore size of 17 nm, respectively.

#### 3.1. Photocharging results using the semi-batch reactor setup

#### 3.1.1. Impact of the type of sacrificial agent

Previously, it could be shown that the amount of stored electrons in photocharged  $TiO_2$  aerogels depends on the concentration of methanol used as sacrificial agent. The intensity of the bluish color increases with increasing concentration of methanol [6].  $TiO_2$  is known to trap electrons close to the surface in presence of a hole scavenger, which goes in line with the formation of  $Ti^{3+}$  states leading to a bluish color of the material with an absorption maximum at 650 nm [21,22,25,26,42]. However, not only the concentration of the sacrificial agent has an influence on the photocharging of  $TiO_2$  aerogels, but also the kind of sacrificial agent as can be seen in Fig. 2. Using the semi-batch reactor, different alcohols were tested, *i.e.*, methanol, ethanol, and isopropanol, as sacrificial agents for their influence on the electron storage ability of the as-synthesized aerogel. The intensity of the hydrogen evolution peaks in the *dark*, after charging for 110 min and the addition of  $H_2PtCl_6$ , in dependence of the sacrificial agent are shown in Fig. 2 (left).

An increase in the hydrogen evolution rate in the dark corresponds with an increasing amount of photostored electrons in the aerogel. Since the amount of added Pt<sup>4+</sup> from the chloroplatinic acid is for all measurements the same, and all Pt4+ is first reduced to Pt0 with stored electrons in the aerogel, a stoichiometric amount of 2 µmol of stored electrons is needed for all measurements to reduce all provided Pt<sup>4+</sup> to Pt<sup>0</sup>. Only the amount of evolved hydrogen in the dark differs, depending on the amount of stored electrons left in the aerogel after the Pt<sup>4+</sup> reduction. This can be quantified by the integration of the hydrogen evolution rate transient [6]. At the end, the amount of stored electrons in the TiO2 aerogel is the sum of the 2 µmol of electrons needed for the reduction of Pt<sup>4+</sup> to Pt<sup>0</sup> of the chloroplatinic acid in the first step, and the amount of electrons needed for the formation of hydrogen in the second step of the dark reduction reaction. The results presented in Fig. 2 clearly show that methanol is the best of the tested sacrificial agents for the electron storage with the as-synthesized TiO2 aerogel. For methanol, an amount of 43.6 µmol of photostored electrons was measured, decreasing to 33.6 µmol of electrons if ethanol is used and to 15.2 µmol of stored electrons for the use of isopropanol as sacrificial agent. This difference in storing efficiency is also visibly assessable by the less intensive bluish color – the amount of Ti<sup>3+</sup> – of the dispersion with isopropanol in the inset photographs of Fig. 2 (left). The amount of photostored electrons of

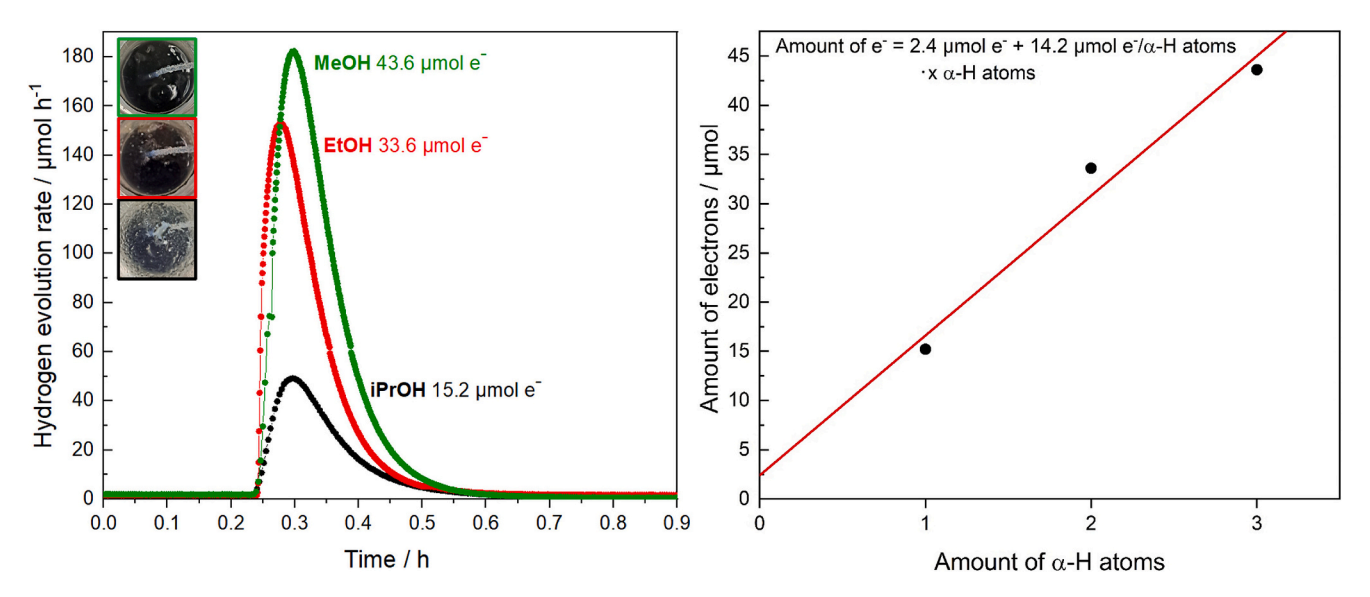


Fig. 2. Hydrogen evolution in the dark for the quantification of stored electrons in the as-synthesized TiO<sub>2</sub> aerogel dependent on the sacrificial agent methanol (green), ethanol (red), and isopropanol (black) with the inset showing photographs of the TiO<sub>2</sub> aerogel dispersions after 110 min irradiation using a 300 W Xe lamp in the semi-batch reactor (left). H<sub>2</sub>PtCl<sub>6</sub> solution was added after 0.22 h to reach 0.1 wt% Pt and H<sub>2</sub> evolution in the dark was measured until no evolution could be detected anymore. The dependence of the obtained amount of stored electrons on the α-H atoms of the used sacrificial agent with the corresponding fit (right).

the as-synthesized aerogel in methanol is higher compared to the previously reported as-synthesized aerogel, which is in accordance to the reported dependence; i.e. an increasing electron storage ability with increasing surface area - the surface area of the herein used aerogel is 642 m<sup>2</sup> g<sup>-1</sup> compared to the previously used aerogel with 600 m<sup>2</sup> g<sup>-1</sup> [6]. The tested three alcohols contain different numbers of protons in the  $\alpha$ -position to the alcohol group ( $\alpha$ -H atoms), increasing from isopropanol with one, to two  $\alpha$ -H atoms for ethanol, and three  $\alpha$ -H atoms for methanol, which goes in line with an increasing polarity from isopropanol<ethanol<methanol. The quantified amount of photostored electrons linearly increases with the number of  $\alpha\textsc{-H}$  atoms in the sacrificial alcohols (Fig. 2, right). During photocharging of the TiO<sub>2</sub> aerogel, hydrogen evolution rates for the three sacrificial agents of up to 0.6  $\mu$ mol h<sup>-1</sup> for ethanol, 0.7  $\mu$ mol h<sup>-1</sup> for isopropanol, and up to 1.8  $\mu$ mol h<sup>-1</sup> for methanol were detected (Fig. S9). These quite small hydrogen evolution rates were expected, as the hydrogen evolution activity decreases with increasing electron storage ability of the TiO2 aerogel, and the as-synthesized aerogel was found to exhibit the best photocharging ability compared to calcined TiO2 aerogels. However, the hydrogen evolution rate in methanol is increased compared to ethanol or isopropanol as sacrificial alcohols. This can be attributed to a photocurrent doubling effect due to the formation of hydroxymethyl radicals, which have a high reduction potential of  $E(\cdot CH_2OH/CH_2O) = -0.95 \text{ V}$  vs. NHE, being high enough for direct injection of an electron to the TiO2 conduction band [43,44]. It was shown that the electron transfer from ethanol and isopropanol to TiO2 is somewhat hindered compared to methanol, which is in line with the lower hydrogen evolution rates detected for ethanol and isopropanol compared to methanol [45]. Additionally, methanol is the best hole scavenger compared to ethanol and isopropanol. Therefore, the recombination rate of electrons and holes in the TiO<sub>2</sub> aerogel is reduced and the amount of stored electrons is increased if methanol is used as sacrificial alcohol instead of ethanol and isopropanol. This effect can be further explained with the oxidation potentials of methanol, ethanol, and isopropanol, which become more positive in the order of methanol>ethanol>isopropanol [46].

#### 3.1.2. Impact of the light intensity and irradiation time

The photon flux (light intensity) and irradiation times are important operating parameters for the photocharging. Dispersions of the as-

synthesized  ${\rm TiO_2}$  aerogel in aqueous methanol solution were investigated, since methanol was shown to be the best sacrificial agent. For all measurements of the photon flux dependence tests, the same 300 W Xe lamp was used for all irradiations; only the reactor was equipped with different neutral density filters to prevent an influence of the light source on the results. Fig. 3 shows the results for the dependence of the photocharging of the aerogel on the photon flux. The hydrogen evolution peaks in the *dark* show increasing hydrogen evolution rates with increasing photon flux during photocharging.

The corresponding amounts of photostored electrons in the  ${\rm TiO_2}$  aerogel reaching values of 17.4 µmol of electrons after an irradiation time of 110 min with a photon flux of 0.324 µmol s $^{-1}$  of the 300 W Xe lamp, increasing up to 43.6 µmol of electrons for a photon flux of 1.176 µmol s $^{-1}$ . A linear dependency of the amount of stored electrons in relation to the photon flux is observed (Fig. 3 (right)). In conclusion, the electron storage ability of the as-synthesized  ${\rm TiO_2}$  aerogel increases linearly with the photon flux. The hydrogen evolution rates during the photocharging of the aerogel with the 300 W Xe lamp in Fig. S10 also demonstrate a linear dependence of the maximum hydrogen evolution rate of the aerogel on the photon flux.

Irradiating the aerogel with 1.176  $\mu$ mol s<sup>-1</sup> of the 300 W Xe lamp, but adjusting the irradiation time from 10 min up to 12 h, results in a different dependency shown in Fig. 4. The amount of stored electrons increases up to an irradiation time of 4 h. After 4 h, the amount of stored electrons does not increase anymore and remains almost constant (Fig. 4, right). Thus, the as-synthesized TiO<sub>2</sub> aerogel is already fully charged after 4 h of irradiation time.

The hydrogen evolution during the longest irradiation time of  $12\,h$  is shown in Fig. S11. Interestingly, the hydrogen evolution rate does not exhibit a constant steady-state rate after 4 h, however increases during the whole irradiation time. Longer irradiation times were not tested for the investigation, since the focus of the work is on the electron storage, which stabilized after 4 h.

# 3.1.3. Cyclability and persistence of photocharging

Cyclic photocharging was investigated with the 300 W Xe lamp and a photocharging time of 110 min, followed by hydrogen evolution detection in the *dark* until the hydrogen evolution decreased significantly. Afterwards, the sample was irradiated again, and the cycle was

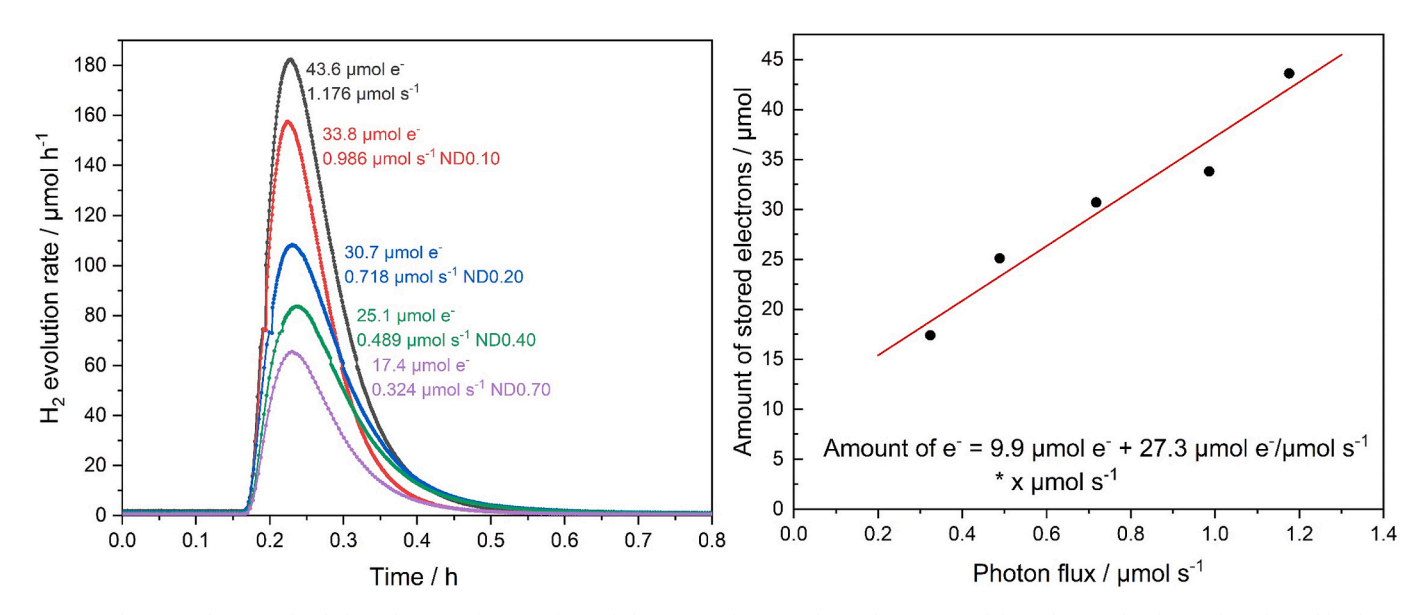
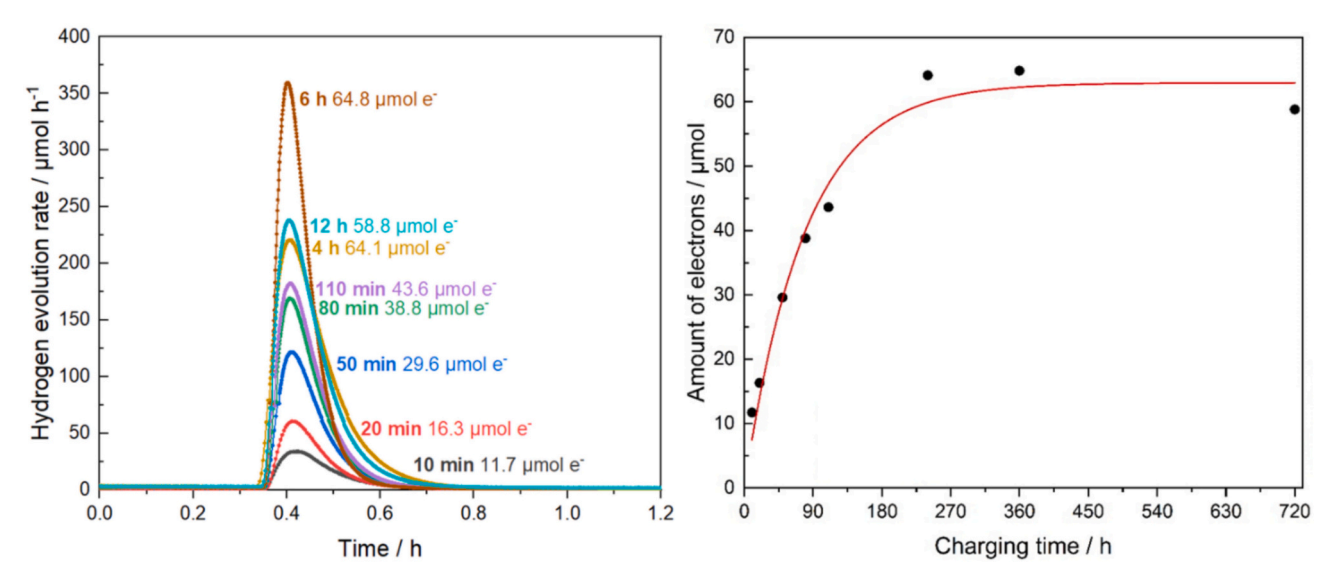


Fig. 3. Hydrogen evolution in the *dark* for the quantification of stored electrons in the as-synthesized TiO<sub>2</sub> aerogel dependent on the photon flux adjusted by the use of a 300 W Xe lamp and the continuous gas-flow batch reactor equipped with different neutral density filters; no filter (gray), ND0.10 filter (red), ND0.20 filter (blue), ND0.40 filter (green), and ND0.70 filter (purple) after an irradiation time of 110 min (left). H<sub>2</sub>PtCl<sub>6</sub> solution was added after 0.15 h to reach 0.1 wt% Pt and H<sub>2</sub> evolution in the *dark* was measured until no evolution could be detected anymore. The dependency of the obtained amount of stored electrons on the photon flux with the corresponding fit (right).



**Fig. 4.** Hydrogen evolution in the *dark* for the quantification of stored electrons in the as-synthesized TiO<sub>2</sub> aerogel as function of the irradiation time with a 300 W Xe lamp using the semi-batch reactor (left). H<sub>2</sub>PtCl<sub>6</sub> solution was added after 0.35 h to reach 0.1 wt% Pt and H<sub>2</sub> evolution in the *dark* was measured until no evolution could be detected anymore. The dependency of the obtained amount of stored electrons on the irradiation time with the corresponding fit (right).

repeated. The results are shown in Fig. 5. Similar to already presented results, the hydrogen evolution rate increases during the charging. The maximum of the hydrogen evolution rate after 110 min charging also increases slightly over the first 5 cycles and decreases afterwards slightly for the 6th and 7th cycle. Even in the *dark*, hydrogen evolution is detected after every charging step for several hours, which is particular obvious after the last charging step. After the last charging step, the bluish color of the aerogel dispersion remained even after 7.5 h of discharging.

The enduring persistence of the color and the hydrogen evolution in the dark until the aerogel is completely discharged is further documented in Fig. S12 together with photographs of the aerogel dispersion after different times of photocharging for 110 min. The charging of the aerogel and thus the  ${\rm Ti}^{3+}$  states persist for more than 24 h. The aerogel is completely discharged after 27 h, which is indicated by the same colorless appearance of the dispersion as before the photocharging was started. This period is in line with an end of the hydrogen evolution in

the *dark*. The long persistence of the charges as well as the cyclability of the charging is advantageous for on-demand solar battery applications of such aerogels.

#### 3.2. Results using the capillary reactor

#### 3.2.1. Capillary materials selection

To identify the most suitable capillary material for photocharging applications, three polymeric capillaries—PFA, FEP, and PVDF—were evaluated under standardized conditions. Each material was tested using a photocharging protocol consisting of 6 h of irradiation with eight 365 nm UV-LEDs (total electrical power: 18.8 W) and a pumping rate of 10 mL/min.

It was observed that TiO<sub>2</sub> (titania) could not be charged in PFA and FEP capillaries. Studies in controlled atmosphere (argon and air) revealed that air diffuses through these capillaries, causing a discharge of the titania aerogel, probably because of the oxygen reduction

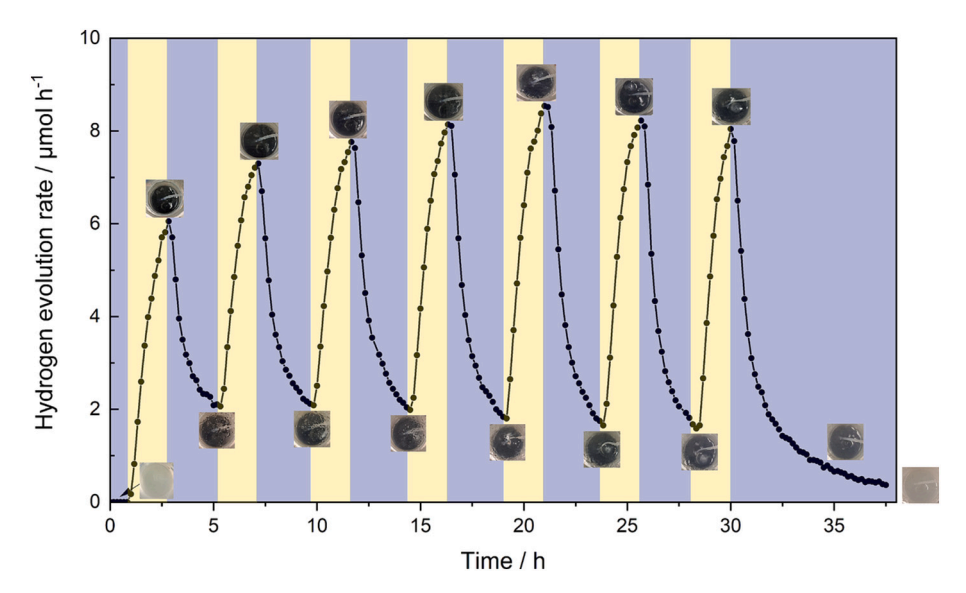


Fig. 5. Hydrogen evolution rate during periodic photocharging cycles of TiO<sub>2</sub> aerogel in the semi-batch reactor with 110 min charging steps under a 300 W Xe lamp (yellow). Hydrogen evolution in the *dark* (blue) was monitored until a significant decrease occurred before each subsequent charging step. Insets show aerogel dispersion at different stages of the experiment.

reaction. Air permeability of FEP, PFA and PVDF film are 2900, 1150, and 7 cm³ m $^{-2}$  d $^{-1}$  bar $^{-1}$ , respectively [47]. In addition, oxygen permeability for FEP, and PVDF was reported as 1200, and 20 cm³ m $^{-2}$  d $^{-1}$  bar $^{-1}$ , respectively [47]. Considering the higher permeability of PFA and FEP in combination with a long capillary and thus a large surface area, significant oxygen intake can occur and reverse photocharging. Due to the superior properties of PVDF in preventing oxygen diffusion, this material was selected for further tests. PVDF also meets the requirement to be transparent for UV light, rendering it an excellent choice for the photocharging capillary reactor. To minimize the influence of potential oxygen permeation into the reactor, the reactor was operated with 1 bar overpressure.

#### 3.2.2. Reactor characterization

 ${\it 3.2.2.1.} \ \ {\it Extinction coefficient.} \ \ {\it Within the limits of the Beer-Lambert law}$ 

$$D_{10} = \beta_{365\;nm}\;c\;l$$

the optical thickness  $D_{10}$  depends on the spectral absorption coefficient  $\beta_{365}$ , the loading of the absorbing species c and the optical path length l. To determine the extinction coefficient, the absorbance was measured as function of titania aerogel loading and optical path length as described by Li et al. [41] The results are shown in Fig. S13. An extinction coefficient of 2.98 L g $^{-1}$  cm $^{-1}$  for a wavelength of 365 nm was determined. For higher titania aerogel loadings, the absorbance of light deviates from the linear relation. The inner diameter of the employed capillary in this study was 1/16''. To account for the curvature of the capillary, the optical path length was calculated by dividing the mean hydraulic cross

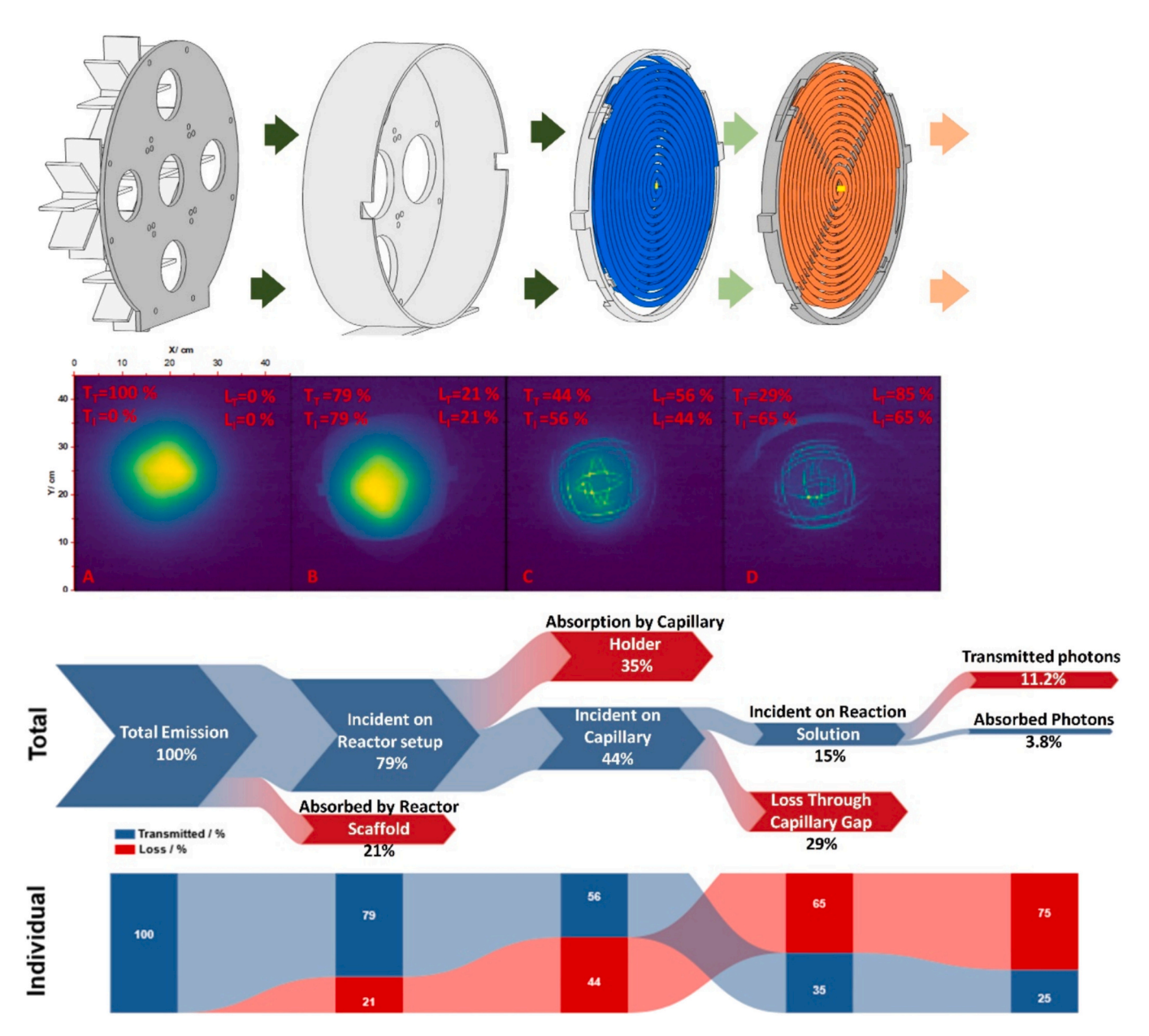


Fig. 6. First row: scheme of the light path through the setup; Second row: Radiometry scans of (a) light source, (b) with reactor housing, (c) with reactor housing, holder and capillary filled with water and methanol, (d) with reactor housing, holder and two-layer capillary filled with methyl orange, total transmission  $T_T = q_t q_0^{-1}$ , where  $q_t$  is the transmitted and  $q_0$  is the incident photon flux and individual transmission  $T_I = q_t q_{0,i}^{-1}$ , where  $q_t$  is the transmitted and  $q_0$  is the incident light on a specific reactor component. Third row: Sankey diagram illustrating the overall photon efficiency within the system. Fourth row: Ribbon graph depicting individual photon losses across the reactor components.

section by the mean diameter of the capillary [48]:

$$1 = \frac{S}{d} = \frac{\pi d^2}{4d} = 1.246 \text{ mm}$$

With a material loading of  $0.66~g~L^{-1}$ , which was used throughout the experiments, the fraction of absorbed or scattered light, f(365~nm), within the capillary was determined to be 24.5 %. Thus, 75.5 % of the total incident photon flux is transmitted through the reactor due to the low loading of catalyst.

3.2.2.2. Radiation field. The incident photon flux on the suspension is an important factor for determining the photocharging efficiency and comparing different reactor types. To avoid detector saturation during radiometric scans, the LED current was reduced to 0.02 A. In the capillary setup, four LEDs were positioned on each side of the reactor. Each LED was individually characterized using a calibrated integrating sphere, resulting in a total photon flux of  $0.37 \ \mu mol \ s^{-1}$ .

A multidimensional radiometric measurement setup developed by Sender et al. [39,40] was used to measure the radiation field of the various reactor configurations (Fig. 6). By combining radiometric measurements with absolute power measurements of each LED with a calibrated integrating sphere, the incident photon flux for the capillary setup could be assessed. The radiation field characterization aimed to elucidate how reactor geometry and material properties influence light utilization efficiency, providing valuable insights for optimizing reactor design.

Photon losses in the reactor were evaluated using two transmission metrics:

 total transmission, defined as the ratio of the transmitted photon flux along a defined light path to the total incident photon flux from the light source:

$$T_{\mathrm{T}} = \frac{\mathbf{q}_{\mathrm{t}}}{q_{\mathrm{0}}}$$

where  $q_t$  is the transmitted and  $q_0$  is the incident photon flux; and.

(2) individual transmission, defined as the ratio of transmitted photon flux to the photon flux incident on a certain reactor part after accounting for individual loss mechanisms occurring on the light path:

$$T_{I} = \frac{q_{t}}{q_{0,i}}$$

where  $q_t$  is the transmitted and  $q_{0,i}$  is the incident light on a specific reactor component. The individual transmission thus reflects the net transmission efficiency after isolating configuration-related losses.

The individual photon loss (L<sub>I</sub>) is defined as:

$$L_{\scriptscriptstyle I}=1-T_{\scriptscriptstyle I}$$

For the case of measurements performed using a capillary filled with concentrated methyl orange, full absorption is assumed and desired and thus any detected transmission is considered a photon loss:

$$L_{\rm I} = T_{\rm I}$$

Analogous to the definition of the transmission, the total photon loss  $(L_T)$  refers to the total photon loss in a given configuration relative to the total photon flux emitted by the light source.

The initial radiometric measurement was conducted with 4 LEDs placed on a reactor cover without side wall (Fig. 6, second row: A),

serving as reference for the other calculations when assuming 100 % transmission. Fig. 6, second row: B shows the radiometry scan of the four LEDs installed within the reactor, including the enclosure. The individual transmission was  $T_{I1} = 79.5 \%$  (equals  $T_{T1}$  in this case), indicating that 20.5 % of photons are lost due to the absorption or scattering by the reactor body. Fig. 6, second row: C shows the radiation field of the reactor with a capillary holder and the capillary filled with water and methanol. The calculated individual transmission for this configuration was  $T_{12} = 56$  %, thus 44 % of the incident photon flux was not available in the capillary. This was considered a photon loss in subsequent calculation of the total available photons as these photons are not available for photocharging. Further investigations were conducted by filling the capillary with a methyl orange solution to mimic a fully absorbing solution. The radiometric scans are shown in Fig. 6, second row: D for two-layer capillaries. The photon flux incident in the capillaries can be determined by assuming that all photons entering the reactor were absorbed by the highly concentrated methyl orange solution. The individual transmission of the two-layer capillaries was measured to be  $T_{13}=65$  % in relation to the transmitted photon flux of the reactor with a capillary filled with methanol and water, i.e. 35 % of the remaining photons are absorbed by the methyl orange solution. The high degree of transmission is attributed to the gap between the capillary and capillary walls. These values were also considered as photon losses in the subsequent calculation of total photons.

The total photonic efficiency, *i.e.* the efficiency to guide photons from the light source to the reaction solution, can be calculated from the efficiencies determined from the radiometric scans with the following equation:

$$\eta_T = T_{I1} \times T_{I2} \times (1-T_{I3})$$

$$\eta_\text{T}=0.15$$

By considering the extinction of the light within the suspension, the total efficiency of the whole setup can be calculated by the following equation:

$$\eta_T \times f(365 \text{ nm}) = 0.038$$

Based on the characterization of the reactor setup, the photon flux available for photocharging was calculated. The LEDs used for the capillary setup used a total electric power of 18.8 W. With a calibrated integrating sphere, an electricity to light efficiency of the LEDs of 40 % was determined, yielding an optical power of 7.5 W. The emitted photon flux was calculated with the following equation:

$$q = \frac{P\lambda}{hc}$$

where h is Plank's constant  $(6.626 \times 10^{-34} J s)$ , c is the speed of light  $(2.998 \times 10^8 \text{ m s}^{-1})$ , and  $\lambda$  is the wavelength of light in meter. A photon flux of  $22.82 \, \mu \text{mol s}^{-1}$  was calculated to be emitted by the LEDs. The photon flux available for photocharging was calculated by considering the different losses caused by the experimental setup, which is illustrated in Fig. 6.

The total photon flux, which could potentially lead to photocharging is  $0.87~\mu mol~s^{-1}$  which is 3.8~% of the total emitted photons.

## 3.2.3. Photocharging results in capillary reactor

Fig. 7 (a) illustrates the light-induced electron storage capability of the titania aerogel suspended in different alcohols including methanol, ethanol, and isopropanol in the capillary reactor. The highest photocharging capacity for the titania aerogel was measured with methanol, followed by ethanol and isopropanol. This trend is consistent with the semi-batch reactor experiments.

The influence of the photon flux on the electron storage capacity of titania aerogel after 6 h photocharging and using the capillary reactor is depicted in Fig. 7 (b). The amount of stored electrons increases with the

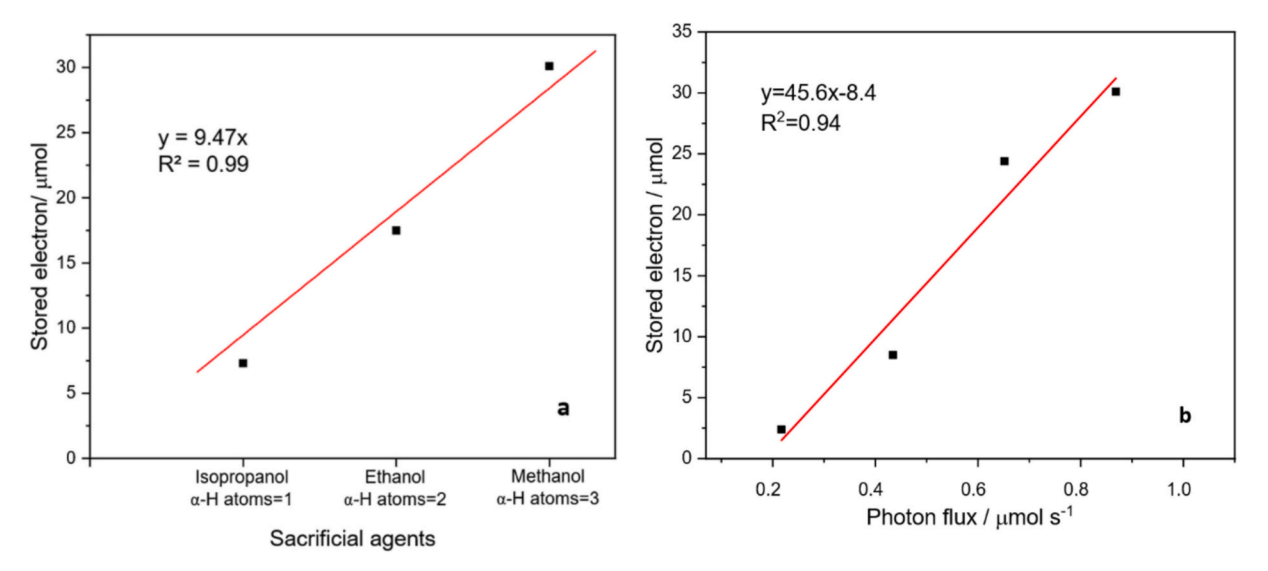


Fig. 7. (a) Photocharging of titania aerogel in the capillary reactor with different sacrificial agents after 3 h irradiation using four 365 nm LEDs. (b) Effect of incident photon flux on photocharging after 6 h irradiation under identical conditions. Photostored electrons were quantified via H<sub>2</sub> evolution after H<sub>2</sub>PtCl<sub>6</sub> addition in the dark.

incident photon flux, which is in line with the results of the semi-batch reactor setup. This correlation implies that the equilibrium concentration of charges is influenced as the rates of generation of the photocharges and the recombination depend on the incident photon flux in a different way. A longer photocharging duration was selected for the capillary reactor, as using the same 110-min photocharging time used for the semi-batch reactor resulted in a significantly lower amount of stored electrons, leading to increased experimental error.

Photocharging was studied for different irradiation times of 40, 80, 110, and 360 min in the capillary reactor. With the total amount of photons incident on the reactor, which can be determined from the

photocharging time and the incident photon flux, the photonic efficiency can be calculated with the following equation:

$$\xi = \frac{amount\ of\ stored\ electrons}{amount\ of\ incident\ photons}$$

The number of stored electrons increases with the irradiation time but levels off with longer irradiation times, as an equilibrium between charging and discharging is reached (Fig. 8). Discharging could occur by the competing hydrogen evolution reaction or the presence of oxygen in the reactor due to diffusion through the capillaries (s. above). This result can also be an explanation for the linearly increasing hydrogen

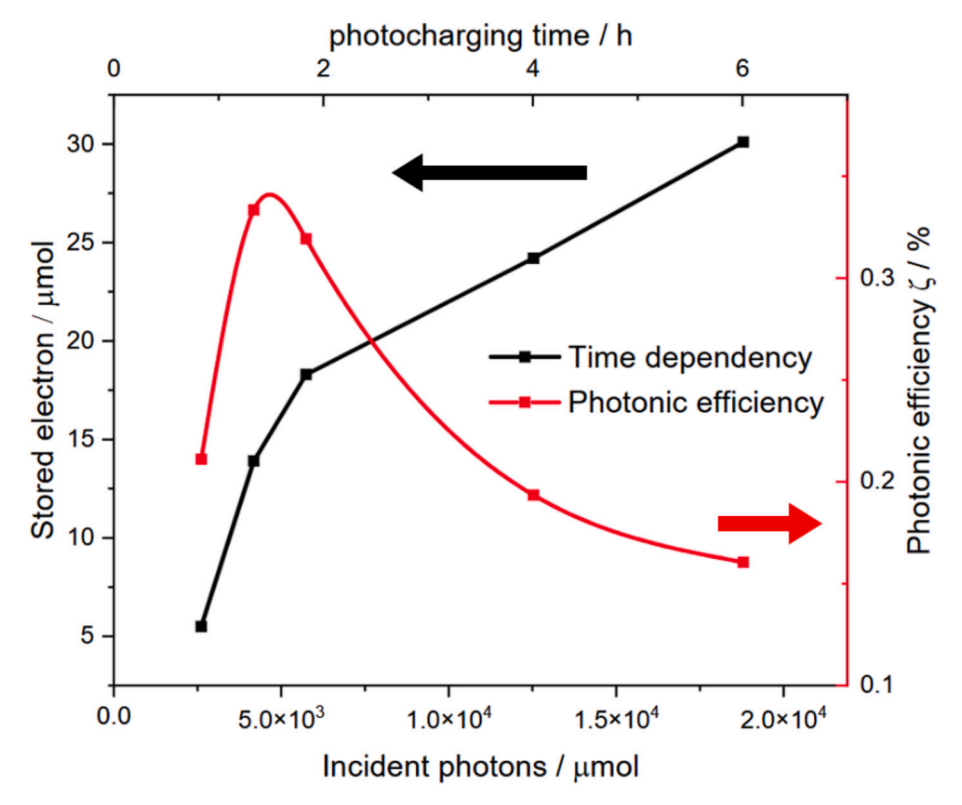


Fig. 8. Photocharging time dependency of electron storage and efficiency of photocharging of the as-synthesized titania aerogel.

evolution rate observed in the experiment with a 12 h irradiation time (Fig. S9).

Periodic photocharging experiments were carried by 3 h photocharing before the LEDs were switched off and the system was operated without irradiation until hydrogen detected by the GC decreased significantly. Subsequently, the lamps were switched on again to start a new photocharging cycle. Fig. 9 shows the detected transient hydrogen evolution. The hydrogen evolution rate increases with time during each cycle and decreases once the lamps were switched off. Notably, the maximum hydrogen evolution rate increased with each successive cycle of photocharging and discharging. The observed trends are similar to the trends observed for the semi-batch reactor.

# 3.3. Comparison of the photocharging efficiency in the semi-batch and the capillary reactor

Given the fundamental design differences between the semi-batch and the capillary reactors, particularly the different light sources and geometrical reactor designs, a suitable method to objectively compare the photocharging performance is imperative, although many qualitative results are very similar. This can be achieved by evaluating performance in relation to the incident photon fluxes and photon irradiance available in each reactor setup.

From spectral irradiance measurements the optical power and eventually the incident photon flux provided within the UV range ( $\lambda$ 420 nm) was calculated for the semi-batch reactor. The semi-batch reactor, equipped with a 300 W xenon lamp, received a photon flux of 1.17 µmol s<sup>-1</sup> within the UV range. In comparison, a photon flux of about 3.54 µmol s<sup>-1</sup> was incident on the capillary reactor. While the photon flux is higher in the capillary reactor, it has to be considered that 75.5 % of the light is transmitted (see Section 3.2.2.2) and only 0.87 μmol s<sup>-1</sup> of the photon flux could potentially lead to photocharging, approximately 25 % less than in the semi-batch reactor where light is fully absorbed. Despite these relatively small difference in available photon flux in both reactors, the semi-batch reactor demonstrates a notably higher photocharging efficiency compared to the capillary reactor (see Fig. 10 a). Taking the photon flux as basis for a performance comparison, the semi-batch reactor is at least twice as efficient as the capillary reactor.

Beside the photon flux, the photon irradiance, *i.e.*, the area normalized photon flux, is important for the overall performance of photon-induced processes as it eventually influences the volumetric rate of photon absorption.

The semi-batch reactor was operated with a photon irradiance of

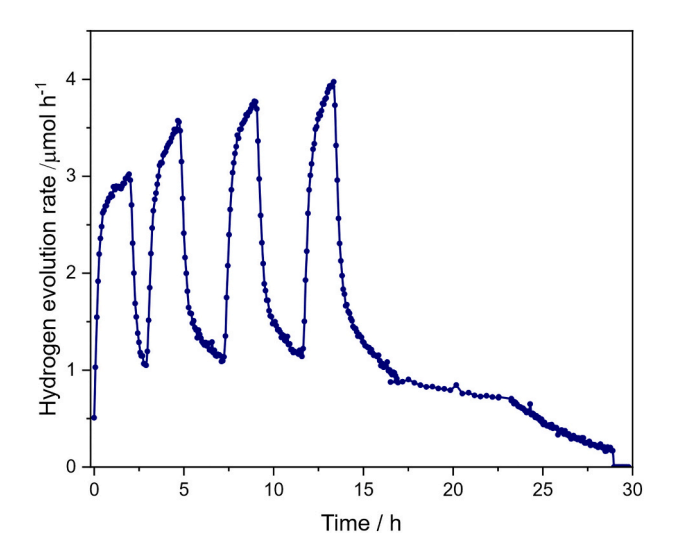


**Fig. 9.** Cycling photocharging of the as-synthesized titania aerogel using the capillary reactor and photocharging times of 3 h with four 365 nm LEDs.

596  $\mu$ mol s $^{-1}$  m $_{\tau}^{-2}$  while the photon irradiance of the capillary reactor was only 72.6  $\mu$ mol s $^{-1}$  m $^{-2}$ . This difference stems from different reactor geometries: the batch reactor has an irradiation window with a diameter of 5 cm, concentrating the light in a small area. In contrast, the capillary reactor has a larger total surface area (diameter of the capillary spiral: 15 cm), resulting in a lower photon irradiance. While the capillary reactor was designed to distribute light across the entire reactor surface, practical limitations lead to gaps between the capillaries (see Fig. S2a), which lead to photon losses. To address this, the projection area of the capillary was calculated by multiplying the diameter with the length of capillary inside the reactor (7.5 m). Calculations indicate that the effective surface area for light absorption is approximately 67 % of the total surface area of reactor.

Since it was found that the photocharging efficiency linearly depends on the photon irradiance, the linear photocharging response observed in the semi-batch reactor was extrapolated to the capillary reactor's photon irradiance of 72.6  $\mu$ mol s $^{-1}$ m $^{-2}$ . The amount of photocharges for the semi-batch reactor at this lower photon irradiance was linearly extrapolated (see Fig. 2) to be 14  $\mu$ mol e $^-$  and thus about 30 % lower than the capillary reactor's performance (18.3  $\mu$ mol e $^-$ ) under identical conditions (see Fig. 10 b). This implies that the significant difference in the photocharging efficiency at higher photon irradiance is due to variations in the equilibrium between the charging and discharging rates.

For better understanding the influence of the photon irradiance on the efficiency of photocharging in the different reactor types, further experiments were conducted by reducing the total volume of the suspension to 25 % of that used in standard experiments. This adjustment accounts for the fundamental difference between two reactors, specifically the total volume of the capillary, as only this is irradiated. The volume of the capillary is approximately 15 mL and with this, only about 10 % of the volume of the suspension (150 mL in typical tests) is under irradiation for normal condition. By reducing the total volume of the suspension to 38 mL with the same catalyst loading (0.66 g L<sup>-1</sup>), the fraction of irradiation volume increases to 40 %. Reducing the total volume of the suspension by about 4 times more than doubles the photocharging rate (Table 1) as well as the amount of electrons stored per 100 mg of aerogel. Increasing the aerogel loading increased the absorbable photon irradiance in the capillary to 145.37 and 290.75  $\mu$ mol s<sup>-1</sup> m<sup>-2</sup> for catalyst loading of 1.32 and 2.64 g L<sup>-1</sup>, respectively, since higher loadings increase the optical density (see Section 3.2.2.2).

After adapting the charging condition to the particularities of the capillary, i.e. higher photon irradiance and reduced dispersion volume, photocharging was found to be faster than in the semi-batch reactor. Photocharging rates were calculated for the capillary and the semi-batch reactors and are summarized in Table 1, Fig. 11. The charging rate in the capillary reactor was 1.25  $\mu mol \; e^- \, min^{-1}, which is more than two times$ higher than in the semi-batch reactor (0.59  $\mu$ mol e<sup>-</sup> min<sup>-1</sup>). An analysis of the photonic efficiencies under optimized conditions revealed a fourfold increase by doubling the catalyst loading in comparison to the standard semi-batch reaction conditions (photonic efficiency increased from 0.21 % to 0.85 %). A further increase in catalyst loading led to a reduction in photonic efficiency. However, the photonic efficiencies remained nearly three times higher than those observed under semibatch reactor conditions. The decline in photonic efficiency is attributed to reaching a saturation point in charge accumulation just before a charging time of 50 min. Commercial anatase nanoparticles (Hombikat UV 100) were employed as a reference to evaluate the electron storage capability in the capillary reactor. Hombikat UV 100 was already investigated in previous studies, showing a less efficient photocharging for comparable crystallite sizes but lower surface area than the aerogel [6]. Under optimized conditions, they exhibited an electron storage capacity of 19.4  $\mu$ mol, corresponding to only 31 % of the total electrons stored in titania aerogel. These results highlight that titania aerogel possesses a remarkable superior efficiency for electron storage compared to conventional anatase nanoparticles.

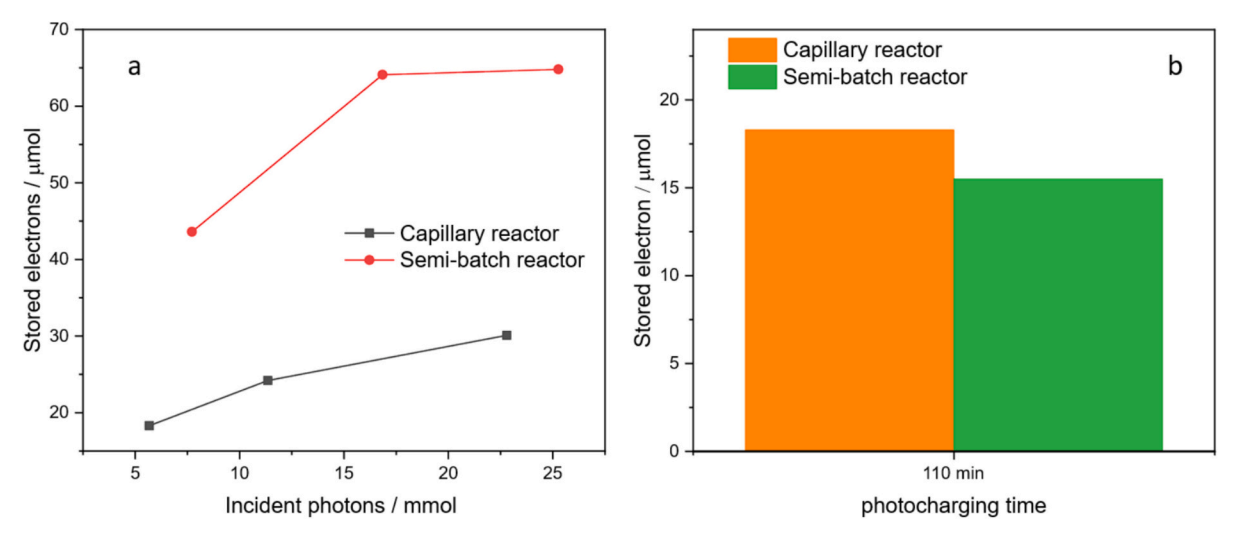


Fig. 10. (a) Photocharging of  $TiO_2$  aerogel in semi-batch and capillary reactors at different times. (b) Comparison of photocharging rates under matched photon irradiance in both reactors.

Table 1

Effect of process parameters on photocharging of titania aerogel in the capillary reactor after 50 min irradiation with eight 365 nm LEDs. Photostored electrons were quantified via H<sub>2</sub> evolution after H<sub>2</sub>PtCl<sub>6</sub> addition in the dark.

Reactor type	Catalyst type	Total Volume/mL	Catalyst mass/mg	Catalyst loading/mg ${\rm L}^{-1}$	Measured electrons/μmol e <sup>-</sup>	Electrons stored in 100 mg aerogel/ $\mu$ mol e $^-$	Photo-charging rate/ µmol e <sup>-</sup> min <sup>-1</sup>	Photonic efficiency/%
Capillary	TiO <sub>2</sub> Aerogel	38	25	0.66	2.54	10.1	0.2	0.38
Capillary	TiO <sub>2</sub> Aerogel	150	100	0.66	5.5	5.5	0.11	0.21
Capillary	TiO <sub>2</sub> Aerogel	38	50	1.32	22.3	44.6	0.89	0.85
Capillary	TiO <sub>2</sub> Aerogel	38	100	2.63	62.6	62.6*	1.25	0.60
Batch	TiO <sub>2</sub> Aerogel	150	100	0.66	29.6	29.6	0.59	0.83
Capillary	Hombikat	38	100	2.93	19.4	19.4	0.38	0.19

Photocharging measurements were conducted using a second batch of titania aerogel, which could store  $31.3 \,\mu\mathrm{mol}\,e^-$ . To consider the differences between the batches, a correction factor of 2 was applied to enable direct comparison with results from the first batch (see Table S1).

# 4. Conclusion

This study investigated the photocharging behavior of as-synthesized titania aerogels in semi-batch and capillary reactors, focusing on key process parameters. Methanol was the most efficient electron donor compared to ethanol and isopropanol, with a linear relationship observed between the number of  $\alpha$ -H atoms and photocharging efficiency. Both photocharging time and photon irradiance strongly influenced performance, with higher irradiance yielding increased electron storage and a linear dependency between photocharging and irradiance.

Photocharging was further transferred from a semi-batch to a capillary reactor. For objective comparison, both reactors were thoroughly characterized. Direct transfer of conditions from the semi-batch system resulted in low performance of the capillary reactor: with low aerogel loading, over 75 % of incident photons were transmitted without contributing to charging. Nevertheless, at identical photon irradiance, 30 % more charges could be stored with the capillary reactor than with the semi-batch reactor. Optimizing aerogel loading and dispersion volume significantly enhanced performance, eventually doubling the photocharging rate of the batch system. Moreover, photonic efficiency in the capillary reactor increased more than threefold after adjustment.

In conclusion, this work provides a comprehensive photo-reaction engineering analysis of titania aerogel photocharging. The results highlight the critical role of radiation field properties - photon flux, irradiance, and volumetric absorption rate - in evaluating and

optimizing performance. These insights demonstrate that scaling photocatalytic processes requires careful consideration of the full experimental setup, forming the foundation for knowledge-driven development of solar-driven and industrial-scale photoreactors.

# Symbols

 $T_{T1}$  % Total transmission of installed LEDs within the reactor setup without holder and capillary

 $T_{T2}$  % Total transmission of installed LEDs within the reactor setup with holder and capillary filled with 10 % v/v methanol

 $T_{T3}$  % Total transmission of installed LEDs within the reactor setup with holder and capillary filled with concentrated methyl orange

 $T_{I1}$  % Individual transmission of installed LEDs within the reactor setup without holder and capillary

 $T_{I2}$  % Individual transmission of installed LEDs within the reactor setup with holder and capillary filled with 10 % v/v methanol

 $T_{I3}$  % Individual transmission of installed LEDs within the reactor setup with holder and capillary filled with concentrated methyl orange

 $\eta_T$  % Total photonic efficiency of guiding photons from the light source to the reaction solution

 $\beta_{365}~{\rm L~g^{-1}~cm^{-1}}~{\rm Spectral~extinction~coefficient}$   $f(365~{\rm nm})$  % Fraction of 365 nm light that is absorbed or scattered

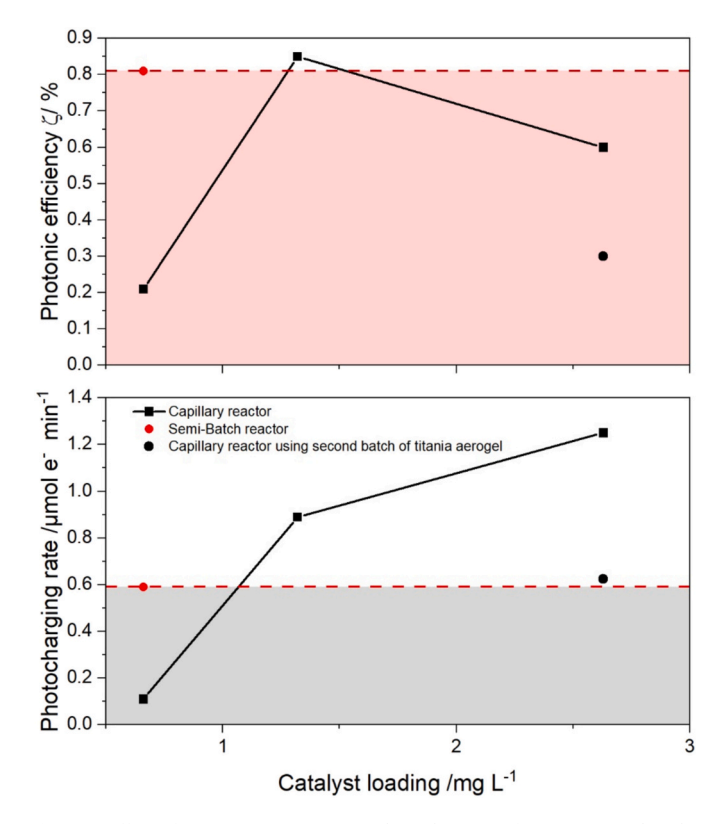


**Fig. 11.** Effect of process parameters on photocharging of titania aerogel in the capillary reactor after 50 min irradiation with eight 365 nm LEDs. Photostored electrons were quantified *via* H<sub>2</sub> evolution after H<sub>2</sub>PtCl<sub>6</sub> addition in the *dark*.

# CRediT authorship contribution statement

Akbar Valaei: Writing - review & editing, Writing - original draft, Visualization, Validation, Software, Methodology, Investigation, Formal analysis, Data curation, Conceptualization. Anja Hofmann: Writing review & editing, Writing - original draft, Visualization, Validation, Methodology, Investigation, Formal analysis, Data curation, Conceptualization. Alexandra Rose: Validation, Investigation, Formal analysis. Paul Kuschmitz: Writing - review & editing, Methodology, Investigation, Formal analysis, Conceptualization. Pascal Voepel: Writing - review & editing, Project administration, Investigation, Funding acquisition, Formal analysis, Conceptualization. Barbara Milow: Writing - review & editing, Supervision, Resources, Project administration, Funding acquisition, Formal analysis. Roland Marschall: Writing - review & editing, Supervision, Resources, Project administration, Methodology, Funding acquisition, Formal analysis. Dirk Ziegenbalg: Writing - review & editing, Validation, Supervision, Resources, Project administration, Methodology, Funding acquisition, Formal analysis, Conceptualization.

# Declaration of competing interest

The authors declare the following financial interests/personal relationships which may be considered as potential competing interests: Barbara Milow, Roland Marschall and Dirk Ziegenbalg report financial support was provided by German Research Foundation. If there are other authors, they declare that they have no known competing financial interests or personal relationships that could have appeared to influence the work reported in this paper.

# Acknowledgements

This work has received financial support from the German Research

Foundation DFG within the Priority Programme 2370 Nitroconversion (project no. 501591928).

#### Appendix A. Supplementary data

Supplementary data to this article can be found online at  $\frac{\text{https:}}{\text{doi.}}$  org/10.1016/j.cej.2025.168924.

#### Data availability

Data will be made available on request.

#### References

- A.L. Luna, F. Matter, M. Schreck, J. Wohlwend, E. Tervoort, C. Colbeau-Justin, M. Niederberger, Appl. Catal. Environ. 267 (2020) 118660.
- [2] V.G. Parale, T. Kim, V.D. Phadtare, H.M. Yadav, H.-H. Park, J. Mol. Liq. 277 (2019) 424.
- [3] J. Kwon, K. Choi, M. Schreck, T. Liu, E. Tervoort, M. Niederberger, ACS Appl. Mater. Interfaces 13 (2021) 53691.
- [4] X. Long, X. Wei, Y. Qiu, Y. Song, L. Bi, P. Tang, X. Yan, S. Wang, J. Liao, Nanotechnol. Rev. 12 (2023), https://doi.org/10.1515/ntrev-2022-0490.
- [5] J.C. Bernardes, G.K. Pinheiro, D. Muller, E. Latocheski, J.B. Domingos, C.R. Rambo, J. Sol-Gel Sci. Technol. 94 (2020) 425.
- [6] A. Rose, A. Hofmann, P. Voepel, B. Milow, R. Marschall, ACS Appl. Energy Mater. 5 (2022) 14966.
- [7] J. Puskelova, L. Baia, A. Vulpoi, M. Baia, M. Antoniadou, V. Dracopoulos, E. Stathatos, K. Gabor, Z. Pap, V. Danciu, P. Lianos, Chem. Eng. J. 242 (2014) 96.
- [8] D.A. Panayotov, P.A. DeSario, J.J. Pietron, T.H. Brintlinger, L.C. Szymczak, D. R. Rolison, J.R. Morris, J. Phys. Chem. C 117 (2013) 15035.
- [9] P.A. DeSario, J.J. Pietron, D.H. Taffa, R. Compton, S. Schünemann, R. Marschall, T. H. Brintlinger, R.M. Stroud, M. Wark, J.C. Owrutsky, D.R. Rolison, J. Phys. Chem. C 119 (2015) 17529.
- [10] C.-C. Lin, T.-Y. Wei, K.-T. Lee, S.-Y. Lu, J. Mater. Chem. 21 (2011) 12668.
- [11] S.K. Parayil, R.J. Psota, R.T. Koodali, Int. J. Hydrogen Energy 38 (2013) 10215.
- [12] R. Moussaoui, K. Elghniji, M. ben Mosbah, E. Elaloui, Y. Moussaoui, J. Saudi Chem. Soc. 21 (2017) 751.
- [13] M.L. Anderson, R.M. Stroud, C.A. Morris, C.I. Merzbacher, D.R. Rolison, Adv. Eng. Mater. 2 (2000) 481.
- [14] N. Hüsing, U. Schubert, Angew. Chemie Int. Ed. 37 (1998) 22.
- [15] S. Alwin, X. Sahaya Shajan, Mater. Renew. Sustain. Energy 9 (2020) 7.
- [16] H. Choi, M. Carboni, Y.K. Kim, C.H. Jung, S.Y. Moon, M.M. Koebel, J.Y. Park, Catal. Letters 148 (2018) 1504.
- [17] S. Sadrieyeh, R. Malekfar, J. Non Cryst. Solids 457 (2017) 175.
- [18] H. Schäfer, B. Milow, L. Ratke, RSC Adv. 3 (2013) 15263.
- [19] S.A. Lermontov, E.A. Straumal, A.A. Mazilkin, A.E. Baranchikov, B.B. Straumal, V. K. Ivanov, Mater. Lett. 215 (2018) 19.
- [20] K.C. Song, S.E. Pratsinis, J. Am. Ceram. Soc. 84 (2001) 92.
- [21] D. Bahnemann, A. Henglein, J. Lilie, L. Spanhel, J. Phys. Chem. 88 (1984) 709.
- [22] H.H. Mohamed, R. Dillert, D.W. Bahnemann, J. Phys. Chem. C 115 (2011) 12163.
- [23] H.H. Mohamed, R. Dillert, D.W. Bahnemann, Chem. Eur. J. 18 (2012) 4314.[24] F.N. Castellano, J.M. Stipkala, L.A. Friedman, G.J. Meyer, Chem. Mater. 6 (1994)
- 2123. [25] H.H. Mohamed, C.B. Mendive, R. Dillert, D.W. Bahnemann, J. Phys. Chem. A 115
- (2011) 2139. [26] H.H. Mohamed, R. Dillert, D.W. Bahnemann, J Photochem Photobiol A Chem 217
- (2011) 271. [27] H.H. Mohamed, R. Dillert, D.W. Bahnemann, J. Photochem. Photobiol. A Chem.
- 245 (2012) 9. [28] I.K. Levy, M.A. Brusa, M.E. Aguirre, G. Custo, E.S. Román, M.I. Litter, M.A. Grela,
- Phys. Chem. Chem. Phys. 15 (2013) 10335.
- [29] N. Murakami, M. Suenaga, R. Deguchi, Inorg. Chem. Commun. 141 (2022) 109585.
   [30] S. Goldstein, D. Behar, T. Rajh, J. Rabani, J. Phys. Chem. A 119 (2015) 2760.
- [31] A. Takai, P.V. Kamat, ACS Nano 5 (2011) 7369.
- [32] D. Kowalczyk, P. Li, A. Abbas, J. Eichhorn, P. Buday, M. Heiland, A. Pannwitz, F. H. Schacher, W. Weigand, C. Streb, D. Ziegenbalg, ChemPhotoChem 6 (2022) e202200044.
- [33] F. Schiel, C. Peinsipp, S. Kornigg, D. Böse, ChemPhotoChem 5 (2021) 431.
- [34] D. Ziegenbalg, A. Pannwitz, S. Rau, B. Dietzek-Ivanšić, C. Streb, Angew. Chemie-Int. Ed. 61 (2022) e202114106.
- [35] P. Jimenéz-Calvo, M.J. Muñoz-Batista, M. Isaacs, V. Ramnarain, D. Ihiawakrim, X. Li, M. Ángel Muñoz-Márquez, G. Teobaldi, M. Kociak, E. Paineau, Chem. Eng. J. 459 (2023) 141514.
- [36] S.D.A. Zondag, J.H.A. Schuurmans, A. Chaudhuri, R.P.L. Visser, C. Soares, N. Padoin, K.P.L. Kuijpers, M. Dorbec, J. van der Schaaf, T. Noël, Nat. Chem. Eng. 1 (2024) 462.
- [37] H. Luo, J. Ren, Y. Sun, Y. Liu, F. Zhou, G. Shi, J. Zhou, Chin. Chem. Lett. 34 (2023) 107782.
- [38] B. Wiedemann, K.M. Carogher, S. Kuhn, D. Ziegenbalg, Chem. Eng. J. 503 (2025) 157987.
- [39] M. Sender, B. Wriedt, D. Ziegenbalg, React, Chem. Eng. 6 (2021) 1601.
- [40] M. Sender, D. Ziegenbalg, React. Chem. Eng. 6 (2021) 1614.

- [41] P. Li, D. Kowalczyk, J. Liessem, M.M. Elnagar, D. Mitoraj, R. Beranek,
- D. Ziegenbalg, Beilstein J. Org. Chem. 20 (2024) 74.

  [42] D. Zywitzki, H. Jing, H. Tüysüz, C.K. Chan, J Mater Chem A 5 (2017) 10957.

  [43] Y.K. Kho, A. Iwase, W.Y. Teoh, L. Mädler, A. Kudo, R. Amal, J. Phys. Chem. C 114 (2010) 2821.
- [44] O. Carp, C.L. Huisman, A. Reller, Prog. Solid State Chem. 32 (2004) 33.
- [45] Y. Tamaki, A. Furube, M. Murai, K. Hara, R. Katoh, M. Tachiya, J. Am. Chem. Soc. 128 (2006) 416.

- [46] J. Lilie, G. Beck, A. Henglein, Ber. Bunsen-Ges. Phys. Chem. 75 (1970) 458.
  [47] H. Fitz, Kunstst.-Germ. Plast. 70 (1980) 27.
  [48] D. Russo, D. Spasiano, M. Vaccaro, R. Andreozzi, G. Li Puma, N.M. Reis, R. Marotta, Chem. Eng. J. 283 (2016) 243.